Electron-Stimulated Desorption of H^+, H_2^+, OH^+, and $H^+(H_2O)_n$ from Water-Covered Zirconia Surfaces

Thomas M. Orlando,* Alex B. Aleksandrov, and Janine Herring

School of Chemistry and Biochemistry and School of Physics, Georgia Institute of Technology, Atlanta, Georgia 30332

Received: January 22, 2003; In Final Form: May 28, 2003

Electron beam induced production and desorption of H^+, H_2^+, OH^+, and $H^+(H_2O)_n$ has been studied from water-covered zirconia surfaces. The proton yield is strongly dependent upon the form of water present with large yields mainly from multilayers or clusters. The high proton kinetic energy distributions and the linear yield vs dose are indicative of proton formation and desorption by 2-hole and 2-hole, 1-electron final states. These localized states are produced either directly or via Auger decay pathways, and desorption occurs from the vacuum surface interface as a result of a Coulomb explosion. The proton yield increases from 80 to 150 K and then drops dramatically as the temperature exceeds 150 K. The increased yield is associated with structural and physical changes in the adsorbed water and longer excited-state lifetimes. The decreased yield is correlated with water desorption. Above 180 K, a small proton signal is observable which we associate with electron-stimulated dissociation of hydroxyl groups present on the zirconia surface. At temperatures above 225 K, this yield drops and gives rise to electron-stimulated desorption of OH^+ ions. H_2^+ is also formed from adsorbed water and involves direct dissociative ionization channels. Some reactive scattering of energetic protons and 2-hole Coulomb interactions produce H_3O^+ and other higher mass clusters such as $H^+(H_2O)_n$, where $n = 2-8$. Though this is a minor channel, it yields information concerning 2-hole screening distances.

1. Introduction

Zirconia (ZrO_2) is a wide-band-gap (>5 eV) transition metal oxide with novel electronic, chemical, and mechanical properties. It has been used in many practical applications that include high-temperature solid-oxide fuel cells, oxygen sensors,[1] substrates for electronic devices,[2] and optical coatings for high-powered lasers.[3] ZrO_2 particles have also been implicated as potentially useful materials for plasma activated[4,5] or radiation-induced surface and interface reactions.[6,7] As an example of the latter, enhanced interfacial energy transfer and elevated yields of hydrogen during γ radiolysis of water on ZrO_2 particle surfaces have been reported.[8,9] Zirconia is the surface barrier coating in some conventional nuclear reactor components[10,11] and the native oxide formed on nuclear fuels packaged in zirconium−alloy claddings. Since these claddings are part of the spent nuclear fuel inventory currently stored in United States Department of Energy interim facilities,[11] fundamental knowledge concerning the physics and chemistry involved in nonthermal (radiation-induced) production of hydrogen at "wet" zirconia surfaces is necessary. This information helps ensure reliable advances in nuclear energy technology and development of safe and defendable nuclear fuel waste storage strategies.

The radiation stability and geometric and electronic structure of thin films of ZrO_2 and pristine yttria-stabilized cubic zirconia have been investigated experimentally using ion-beam bombardment,[12] X-ray photoelectron spectroscopy,[13] and electron- and photon-stimulated desorption.[14,15] These studies indicate that clean ZrO_2 surfaces are relatively stable to bombardment with ionizing radiation. The primary modes of radiation damage involve Auger-stimulated channels and possibly exciton decay at the surface.[14] Both of these processes result primarily in the removal of oxygen from the surface and near-surface region and reduction of the Zr cation charge states. The radiation-produced surface defect sites are very reactive and can lead to the efficient dissociative chemisorption of water and the facile production of surface hydroxyl groups.

Though the interaction of water with metal oxides is a topic of wide concern in the surface science community,[16] there are only a few studies on the chemisorption and physisorption of water on ZrO_2 thin films or single crystals. Studies using zirconia thin films grown on Pt(111) surfaces report several maxima in temperature-programmed desorption spectra that correspond to different water binding sites.[17,18] Fourier transform infrared spectroscopy of polycrystalline grains of monoclinic and tetragonal zirconia show complete removal of nondissociated water from the oxide surface at temperatures above 470 K. Above this temperature only absorption bands corresponding to free surface hydroxyl groups assigned to terminal and tribridged types are observed.[19]

Despite the vast technological and environmental relevance of zirconia, there have been surprisingly few studies on the fundamental properties and reactions of ZrO_2 films and substrates involving water *and* radiation. In fact, no quantitative measurements of the atomic and molecular hydrogen (ionic and neutral) yields from electron-irradiated ZrO_2 surfaces containing chemisorbed or physisorbed water have been reported. As a first step in filling this gap, we have completed experiments on the thermal and nonthermal desorption of water-covered thin films of ZrO_2. Specifically, we have examined the nature of the adsorbed water species and the identities and energy distributions of the electron-stimulated desorption (ESD) products. In section

* Corresponding author. E-mail: Thomas.Orlando@chemistry.gatech.edu. Fax: (404) 894-7452.

10.1021/jp030117k CCC: $25.00
Published on Web 08/12/2003

2, we describe the experimental approach. Section 3 presents our results on the temperature-programmed desorption (TPD) studies and the electron dose, substrate temperature, and water coverage dependencies of the 100 eV ESD cation yields. Discussions of the primary mechanisms leading to cation desorption and the relevance to energy transfer at ZrO_2 interfaces are also presented in section 3. Finally, section 4 contains the summary and conclusions.

2. Experimental Procedure

The experiments were performed in an ultrahigh vacuum chamber specifically designed to examine radiation (electron-beam) effects at water:oxide interfaces. Briefly, the system consisted of an ultrahigh vacuum chamber (base pressure $\sim 2 \times 10^{-10}$ Torr), equipped with a rotatable helium-cooled sample holder, a computer-controlled resistive tungsten sample heater, quadrupole and time-of- flight (TOF) mass spectrometers, a pulsed low-energy electron gun, and a calibrated dosing system. The polycrystalline zirconium sample (99.94% purity) was oxidized by maintaining the sample for several hours at 800 K in the presence 10^{-8} Torr of water vapor or oxygen. This treatment produces a 3−5 monolayer (about 15−30 Å) coverage of zirconium suboxides with an average composition of $ZrO_{1.5}$.[20] At some point, restructuring of this surface oxide forms microcrystals of zirconia (ZrO_2), probably mostly with the cubic structure.[21] The crystalline and structural properties of these and similar films grown on single-crystal substrates have been well characterized.[20−22] At temperatures above 600−700 K, dissociative adsorption of water on the zirconia surface forms a hydroxyl layer[23] that screens zirconium cations in the near-surface region. Since one of our goals was to mimic conditions relevant to fuel claddings, we initially dosed at 600 K to ensure that surface hydroxyl groups were always present in our experiments. The water was introduced into the chamber after several freeze−pump−thaw cycles using a standard UHV dosing system. The dose rate and coverages were calibrated relative to known temperature-programmed desorption (TPD) profiles from water adsorbed on Pt(111). TPD measurements were performed using a 1.5 K/s constant temperature ramp and a quadrupole mass spectrometer.

Irradiation of the grounded sample was performed by the pulsed electron beam operated at a 500 Hz frequency. The electron energy, flux, and pulse length were varied over a wide range depending on the purposes of the experiment. Typical operating conditions were $\sim 10^{13}$ (electrons/s) during a given pulse or time-averaged currents of $\sim$100 pA (10^{-10} A at an electron gun repetition rate of 500 Hz and a pulse length 200 ns). These fluxes were low enough to preclude surface charging and avoided complications due to above surface collision processes. Since we utilized a pulsed electron beam, the ESD of ions was measured by a TOF mass spectrometer with better than unit mass resolution. Emitted ions were usually collected by applying a 100 V pulsed extraction potential to the TOF front lens assembly. The 100 V potential was high enough to ensure a large solid angle and rules out any discrimination against off-normal trajectories or ion angular distribution effects. The extraction pulse was applied just after the end of the electron pulse to avoid the influence of the potential field on the electron energy. All ions were detected using pulsed counting and a transient digitizer, and the high sensitivity of this approach allowed the observation of weak cluster ion signals. To measure accurate kinetic energy distributions of emitted ions, no extraction pulse (i.e. field free conditions) was used. The sensitivity using this approach is reduced, and thus only the velocity distribution of the departing protons was measured under field-free conditions.

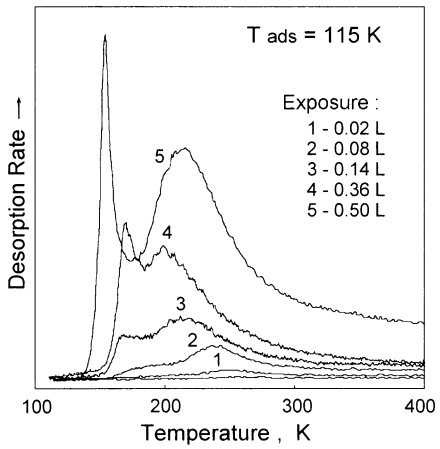

Figure 1. Temperature-programmed desorption of water from the surface of zirconia. The substrate heating rate was 1.5 K/s.

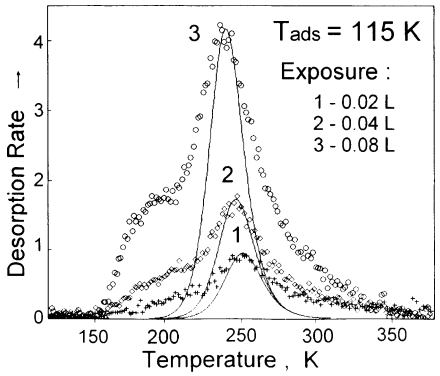

Figure 2. Temperature-programmed desorption spectra of the high-temperature feature shown in Figure 1. The solid lines are fits to the data using the Polayni−Wigner equation for second-order desorption. Assuming a normal prefactor of 10^{13} (ML s)$^{-1}$, the fit yields a desorption activation energy of 58 kJ/mol.

3. Results and Discussion

A. Nature of Adsorbed Water: Temperature-Programmed Desorption. The structure and form of adsorbed water at submonolayer coverage, especially at the surface of such a complex system as hydroxylated zirconia, is not well understood. In an effort to examine this, we carried out TPD studies of water deposited on ZrO_2 surfaces at 115 K. These results are shown as a function of exposure (coverage) in Figures1 and 2. At water exposures less than 1 langmuir, well-defined desorption features are observed at substrate temperatures between 170 and 200 K and 200−300 K. As the water coverage increases, the 200−300 K feature broadens and the peak shifts to lower temperature. The feature at 170−200 K also shifts and develops a profile that is characteristic of ice or multilayer desorption.

We note that the TPD spectra obtained from other metal-oxide single-crystal surfaces reveal several common features. Specifically, a similar desorption feature between 200 and 300 K is observed in the TPD of water from MgO(100)[24] surfaces and TiO_2(110).[25] In the case of MgO, the uptake was precursor mediated and the TPD features were independent of the defect density. The desorption rates were interpreted in terms of the presence of a chemisorbed state(s) kinetically coupled to defects rather than extensive dissociative adsorption. The low-temperature features also shifted to lower temperature as observed in our experiments.

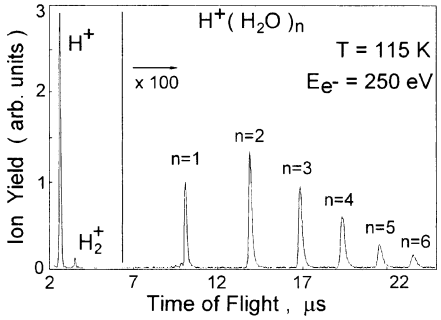

Figure 3. Time-of-flight mass spectra of the cations desorbed during the pulsed electron beam irradiation of water-covered zirconia surfaces. Incident electron energy: 250 eV. Note the cluster ion yield has been multiplied by a factor of 100 compared to H^+. Similar TOF spectra are obtained at lower energies such as 50 and 100 eV. The water dose was 40 L, and the substrate temperature was 115 K.

The line shapes and the coverage dependencies of the features in TPD spectra are often used to infer the molecular nature of adsorbates. TPD peaks that shift to a lower temperature with coverage can be indicative of second-order kinetics but are often interpreted as first-order kinetics with coverage dependent energetics. Figure 2 shows a simple analysis of the data for the high temperature state using the Polanyi−Wigner equation for second-order kinetics, and the fit (shown by the solid line) is satisfactory. Assuming a normal prefactor of 10^{13} (ML s)$^{-1}$, the fit yields a desorption activation energy of ∼58 kJ/mol, in accord with previous TPD studies of water on metal oxides.[24,25] We also interpret our data in terms of molecular desorption of a chemisorbed state which is kinetically coupled to defects or other chemisorbed water molecules. The desorption probability of this chemisorbed state increases with coverage due to a reduced coupling with the surface and an increased intraadsorbate interaction. Since we do not know the number density and specific types of defects present, we have not attempted to model this complicated kinetic coupling. We interpret the gradual shift of the feature near 200 K to a peak near 170 K as the initial growth of a bilayer phase and a concomitant growth of 2-D clusters. At the highest coverage, 3-D clusters can form prior to the completion of the formation of the monolayer and bilayer phases.

B. Electron-Stimulated Desorption of Ions from Water-Covered ZrO2 Surfaces.

B.1. Time-of-Flight Distributions and Dose Dependence of Cation Yields. A typical TOF spectrum of the cations produced and desorbed during 250 eV electron beam bombardment of a water covered zirconia surface is shown in Figure 3. A small signal is present to $n = 8$ (not shown). This TOF spectrum is very reproducible providing the samples received doses that exceed 1 langmuir. The ESD ion yield is clearly dominated by protons, the second most abundant product is H_2^+, and the least abundant species are the protonated cluster ions. Although the cluster ion yield is low, the distribution is typical for amorphous ice or amorphous clusters supported on rare gas substrates.[26] As discussed further below, their size distribution and general presence is indicative of the importance of ionization (electron−hole production) and the distance range the holes can travel in amorphous water.

The proton yields were high enough to allow measurements as a function of electron beam flux over a useful dynamic range under completely field free (grounded extraction grid and sample) conditions. These TOF spectra, which are presented in Figure 4, can be converted into kinetic energy distributions $I(E)$ using the Jacobian transformation $I(E) = I(t)t^3/(mL^2)$. An

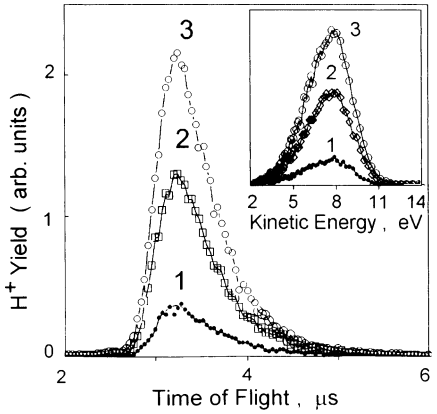

Figure 4. Time-of-flight velocity distribution of H^+ measured under field-free conditions. The incident electron energy used is 120 eV, and the water dose was 20 Langmuir. The numbers 1, 2, and 3 corresponds to electron fluxes during the pulse of 5×10^{12}, 1×10^{13}, and 1.5×10^{13} e/cm^2 s, respectively. The velocity distributions have been converted to kinetic energy distributions (see text). Note the distributions are independent of the flux.

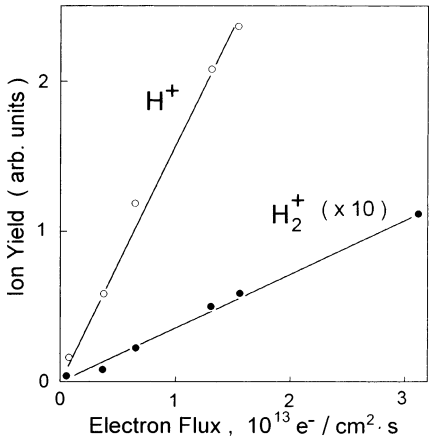

Figure 5. Electron flux dependence of the H^+ and H_2^+ yields obtained by integrating the TOF spectra such as those shown in Figure 4. Note the H_2^+ yield is multiplied by a factor of 10.

example of the energy distribution is shown in the inset in Figure 4. The shape of this distribution is consistent with previous studies[27,28] and can be described as a superposition of two distributions with different peak energies. Decomposition of the spectrum into two Gaussian components shows that, in addition to the main process resulting in emission of protons with an average kinetic energy of ∼7 eV, another less effective process occurs which produces protons with peak kinetic energies near 4−5 eV.

The instantaneous dose rate dependence of the proton yields can be obtained easily by integrating the TOF peak areas obtained under field-free conditions (Figure 4) and/or using a 100 V extraction potential. The latter approach also allows us to determine the dose rate dependence of the H_2^+. The dose rate dependencies of the atomic and molecular hydrogen ion yields are presented in Figure 5, and the yield of both products is clearly linear. Such dose rate dependencies are indicative of single electron impact events at the surface and rule out contributions from gas-phase collision processes or two-step processes at or within the target. The low signal level for the cluster ions precluded an accurate dose dependence study of these products. However, due to the low incident electron flux, we expect that the cluster ions are produced solely at the surface.

B.2. Temperature Dependence of Cation ESD Yields. Orlando et al. have previously investigated the temperature

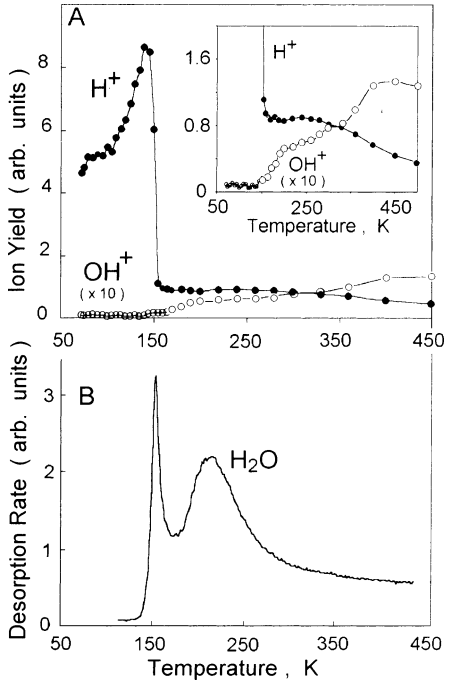

Figure 6. (A) Temperature dependence of the H^+ and OH^+ ESD yield as a function of substrate temperature. The incident electron energy was 120 eV, and the initial water dose at 115 K was 1 langmuir. The inset shows a more detailed comparison of the H^+ (●) and OH^+ (○) ESD yield at higher temperatures. (B) TPD of water on zirconia thin films after 0.5 L exposure in water vapor at 115 K. The feature at 150 K represents the multilayer clusters or aggregates whereas the higher temperature feature corresponds to chemisorbed water species which are likely associated with defects and coadsorbed water molecules (see text for discussion).

dependence of the proton yield from nanoscale ice films[28,29] and demonstrated that the yield is a very sensitive function of the lifetime of excited-state configurations containing a_1 character. The temperature dependence of the proton ESD yields from water covered ZrO_2 is presented in Figure 6A. The yield increases at ~120 K until a maximum is reached at 150 K, and then the yield drops precipitously. Comparison of the temperature dependence of the ESD proton yield to the thermal desorption yield is shown in Figure 6B. The ESD yield increase at 120 K occurs well before the thermal desorption rate becomes appreciable whereas the abrupt drop is directly related to the sublimation and thermal removal of clusters and multilayer water. Orlando et al. associated the yield increase at 120 K to motion and diffusion of intrinsic orientational Bjerrum-type defects which are configurations with missing hydrogen bonds. These defects can be present in layers which exceed the thickness of a bilayer. The diffusion of these defects provides a mechanism for reorientation of surface water molecules and reduces the perturbation of the $4a_1$ level. In terms of the electronic structure effects, this primarily involves the return of atomic p_z character in the localized molecular orbitals of the surface molecules. Since the present results are essentially identical to our previous studies on 50 ML films grown on Pt(111), we invoke the same arguments to explain the results from 80 to 160 K.

An important observation in the water:zirconia system is the weak continuation of the proton signal after the loss of the primary chemisorbed water. The proton signal at high temperature is likely due to the presence of surface hydroxyl groups. In addition, there is the conspicuous onset of nonthermal desorption (i.e. ESD) of a higher mass product which we assign as OH^+. Though the velocity spread precludes ruling out the

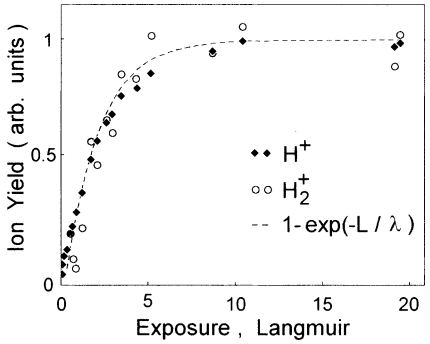

Figure 7. H^+ (♦) and H_2^+ (○) ESD yield as a function of water dose or overlayer thickness (L). The dotted line is a fit using the equation $1 - \exp(-L/\lambda)$, where L is the thickness and λ is the mean-free path of the incident electron. The incident electron energy was 420 eV, and a value of 6 Å was used for λ (see text for further details).

production and desorption of H_2O^+, our previous mass-resolved ESD and PSD measurements of zirconia dosed with small amounts of water revealed solely the presence of OH^+.[14] A direct comparison of the proton and OH^+ yield as a function of temperature is shown in the inset of Figure 6A. There is an obvious correlation between the loss of protons and the increased yield of OH^+ with increasing temperature.

We have previously shown that the ESD of O^+ and OH^+ cations can occur via Auger decay of holes produced in the Zr^{4+} d-band.[14] This is a classic example of the Knotek−Fiebelman mechanism for cation ESD from full valence metal-oxide systems.[30] It is well-known that the strong electron− and hole−phonon coupling typical of wide-band-gap metal-oxide systems increases with temperature.[31] Since much of the surface phonon activity will be in the low-frequency modes associated with the motion of the O−H bond, the hole hopping probability out of this bond will increase. Holes produced in the bulk will also be transported more efficiently to the interface. In addition, the Auger decay rate of a hole produced in the Zr^{4+} d-band may be enhanced. Collectively, all of these processes could lead to more efficient localization of holes in the oxygen 2p level. If the lifetime of these multihole localized states exceeds those of the 2-holes in the OH bond, an increased OH^+ yield will result. Since the terminal hydroxyl groups are the primary source of the protons at high temperatures, an increased yield of OH^+ must cause a reduced yield of the protons.

B.3. Film Thickness Dependence of Proton ESD Yields. Studies by Orlando et al. have also demonstrated that the proton ESD yield is very dependent upon the phase and thickness of water overlayers.[32] The weak phase dependence was mainly related to the number of dangling bonds present at the surface whereas the thickness dependence was more complicated and was related to 2-hole localization probabilities, the mean roughness of the film, and the reactive scattering of the outgoing proton. The thickness dependence of the ESD of protons from water dosed zirconia surfaces is shown in Figure 7. Protons are observed at the lowest coverage, and as discussed above, the yield never goes to zero, even at the highest temperatures studied. The protons at very low coverage are due to the presence of surface hydroxyl groups produced as a result of dissociative chemisorption. The yield increases dramatically as the water coverage increases and then reaches a limit that is independent of dose and coverage. Since proton ESD generally requires the formation of a 2-hole localized state on the terminal water sites (see discussion on the mechanism below), the image interaction governs the production in the very low-coverage (<1 BL) regime. Above this regime, the proton yield is dominated by the relative coverage and probability of depositing energy

into the water clusters or aggregates vs the underlying substrate. This can be qualitatively modeled with the following simple expression $Y = 1 - \exp(-L/\lambda)$, where λ is 6 Å, the approximate inelastic mean free path of 100−400 eV electrons in water,[33] and L is the overlayer thickness. The dotted line in Figure 7 is the fit using this equation.

The thickness dependence of the normalized H_2^+ yield is also shown in Figure 7, and it is essentially identical to that of the proton yield. Though the yield of the H_2^+ is more than a factor of 50 smaller than the H^+ yield, the strong similarities in both the dose and thickness dependencies indicates that similar and related processes are involved in their formation and desorption. This is discussed in more detail in section B.4.2.

B.4. Mechanisms of Cation ESD from Water-Covered ZrO_2 Surfaces. Prior to discussing the mechanisms leading to ESD of cations from wet ZrO_2 surfaces, we first summarize some the relevant information concerning the electronic structure of ice. The ground state of an isolated water molecule is $(1a_1)^2(2a_1)^2(1b_2)^2(3a_1)^2(b_1)^2$, where the a_1 orbital is essentially the oxygen (1s) core level, the $2a_1$ and $1b_2$ orbitals are primarily involved in O−H boding, and the $3a_1$ and $1b_1$ are primarily nonbonding The two lowest lying unoccupied orbitals are the $4a_1$ and $2b_2$. The $4a_1$ level is strongly antibonding and is mixed with the 3s Rydberg state. The electronic structure of ice is similar to that of gas-phase water; however, the following important differences have been noted: (i) The high-lying $2b_2$ orbital is apparently replaced by a conduction band. (ii) The conduction band is very narrow and rather ill-defined with a band minimum roughly 1 eV below the vacuum level. (iii) The valence levels are shifted slightly in energy, and bands containing a_1 character have the largest dispersion (the $1b_1$ and $1b_2$ levels are basically dispersionless). (iv) The $4a_1$ level, which is below the conduction band-edge, is localized (excitonic) and maintains dissociative character.[28]

B.4.1. Protons. The very strong proton signal has been studied in detail, and it is well established that proton desorption involves the production of 2-hole states which Coulomb explode directly at the surface. Since population of the $4a_1$ level also contributes a dissociative force, several of these 2-hole states are thought to be screened or involve population of this level. The primary threshold energy for producing and desorbing protons in this study is ∼22 eV, and a second threshold is observed around 40 eV. These threshold energies are identical with our previous studies[14,28] and have been obtained for doses greater than 1 L. The ∼22 eV threshold has been assigned to the $(1b_1)^{-2}(4a_1)^1$ and $(3a_1)^{-1}(1b_1)^{-1}(4a_1)^1$ final states whereas the 40 eV threshold was associated with the $(3a_1)^{-2}(4a_1)^1$, $(3a_1)^{-1}(1b_2)^{-1}(4a_1)^1$, and $(1b_2)^{-2}(4a_1)^1$ states. Excitation energies greater than ∼70 eV have also been observed to yield very energetic protons due to the formation of the $(2a_1)^{-2}$ final state. The threshold energy for proton ESD from metal hydroxides is also near 22 eV and is associated with an initial ionization of the oxygen 2s level which Auger decays. All the incident electron energies used in this study exceed all the experimentally observed threshold energies for creating protons. Since the $1b_1$ and $3a_1$ orbitals rehybridize and participate strongly in hydrogen bonding in ice, valence holes in these levels should be delocalized. This will cause a reduction of the final state lifetimes and reduced proton yields. However, the more localized $(1b_2)^{-2}(4a_1)^1$ and $(2a_1)^{-2}$ configurations should have longer lifetimes and likely dominate the formation and desorption of protons.

Configuration interaction calculations on the energetics and forces characterizing the important 2-hole, 1-electron and 2-hole final states relevant to this study have been carried out,[27,34] and the summary of these results are listed in Table 1. The proton kinetic energy arises primarily from the Coulomb repulsion energy and thus the localized $(1b_2)^{-2}(4a_1)^1$ and $2a_1^{-2}$ configurations yield protons with the highest kinetic energies. Inspection of Figure 4 shows that most protons that leave the surface as a result of 120 eV electron bombardment possess kinetic energies greater than 5 eV. This result is consistent with assigning the $(1b_2)^{-2}(4a_1)^1$ and $2a_1^{-2}$ configurations as some of the primary excited states governing proton ESD.

TABLE 1: Excitations of Water Leading to D^+ Emission[28,34]

excitation energy (eV)	valence config	D^+ kinetic energy (eV)
21−25	$3a_1^{-1}1b_1^{-1}4a_1^1$	0−4
26−31	$1b_1^{-2}4a_1^1$	4−7
31−36	$3a_1^{-2}4a_1^1$	1−4
∼70	$2a_1^{-2}$	>7

B.4.2. Molecular Hydrogen Ions. The 2-hole, 1-electron or 2-hole final states discussed above can also decay via other pathways that competes with the formation of protons. These decay channels involve the formation of $H_2^+ + O$ or $H_2^+ + O^+$, respectively. This complicated process has been reported in electron-impact studies of gas-phase water, albeit with a very low contribution ($\sim 2 \times 10^{-3}$) to the branching fraction observed in the time-correlated dissociation of doubly ionized states of water.[35] This channel was not observable in single-photon studies using He IIα (30.4 nm) and He IIβ (25.6 nm) radiation.[36] Thus, autoionizing triplet states that are not accessible in single photon studies may be involved. In fact, a more recent study on the multiphoton ionization and dissociation of water has revealed the presence of an excited ion states that decay to form H_2^+ directly.[37] Specifically, H_2^+ was observed only after the absorption of four 532 nm photons by the initially produced water ions. The final state energy was approximately 22 eV. The pathways for the formation of H_2^+ ($X\ ^1\Sigma_g^+$) were attributed to nonadiabatic dissociation via the $X\ ^2B_1$ or excited $B\ ^2B_2$ state of the water parent ion. These are the only states within the doublet system of electronic states of H_2O^+ that have H_2^+ ($X\ ^1\Sigma_g^+$) as a dissociation product.

We note that the flux dependence shown in Figure 4 indicates that H_2^+ formation involves a single electron-impact event. This is obviously the case for direct formation via the molecular elimination channel. It is also consistent with reactive scattering of energetic protons providing this involves a preformed dimer (or higher coordination) configuration. Since all terminal water molecules on an ice surface must be hydrogen bonded to at least one or two water molecules, this criteria is always fulfilled. However, the very strong polarization interactions and solvation forces associated with condensed phase targets introduce energetic barriers for desorption of H_2^+. We therefore favor dissociative ionization involving direct molecular elimination as the primary channel for the production and desorption of H_2^+.

B.4.3. Protonated Cluster Ions. The H^+ and H_2^+ ions are created via dissociative ionization and Coulomb repulsion involving 2 holes localized within the same molecule. The formation and desorption of the cluster ions also likely result from Coulomb repulsion; however, in this case, the valence holes may be on separate water molecules but confined within the cluster. It is expected that many of the valence band holes created at the incident electron energies used in this study are produced via Auger decay. These holes can move rapidly within the bands, and previous PSD and ESD studies clearly showed that holes in bands containing a_1 character experienced the greatest dispersion or delocalization.[28,38] A later experiment

involving the low-energy H^+ scattering from water overlayers corroborated these previous results.[39] In order for cluster ions to be produced and desorbed, holes must remain localized for approximately 100 fs over the range of the Coulomb forces. Assuming at least two hydrogen bonds (~0.5 eV) must be broken and a polarization potential of 2 eV must be surmounted, we estimate that a hole separation distance of ~<10 Å can result in cluster ion desorption. Distances greater than this will tend to result in efficient screening, a strongly reduced Coulomb field, and little desorption. Therefore, 10−12 Å is a reasonable estimate of the hole screening distance in amorphous water and implies that desorption of hydrated protons is likely dominated by clusters or islands which are smaller than 1.0−1.2 nm. Though we have no direct information regarding the shape and size distribution of the clusters and structures present on the amorphous and porous ice overlayer, it is interesting to note that 1.0 nm is close to the diameter for a unit cell in crystalline ice which contains 6 water molecules in a hexagonal lattice arrangement.

It is useful to compare our observed cluster distribution to the cluster size distribution measured during the formation of the chemisorbed phase of water on metal surfaces.[40] At very low coverage, the initial interaction of water molecules is dominated by the water−surface interaction. However, as the coverage increases, the interaction between the water molecules increases and the strong ion−dipole coupling leads to the facile formation of dimers. These are present in large quantities and diffuse freely until trimers and higher order clusters are formed. At equilibrium, a statistical distribution of cluster sizes exists with the weighting toward smaller cluster sizes. Ultimately, the diffusion of higher mass clusters (i.e. hexamers) will be self-limited and the clusters will interact more strongly with the surface forming the template for multilayer growth. If the multilayer growth forms a perfect crystalline solid, the surface water molecules will have a coordination number of 3. At the temperatures used in our studies (<115 K), the multilayer regions are amorphous and should be characterized by a large number of defect sites with coordination numbers less than 3. These terminal configurations will tend to be dominated by dimer and trimer configurations.

C. Relevance to Interfacial Energy Transfer. In view of the valence band structure of zirconia,[23,41] there is the potential for energy transfer to adsorbates such as water. The mechanism for this is complicated and could involve a number of processes that include secondary electron scattering, hole transfer or exciton transfer. As discussed above, ESD of H^+ and H_2^+ from water-covered zirconia requires the formation of a 2-hole localized state on terminal water sites and ESD of protonated cluster ions require 2 holes localized within a nanoscale cluster or a protonated cluster and a hot hole. We note that the 30 Å thick zirconia films examined were roughly the thickness necessary to screen the underlying zirconium image interaction but do not appear to be thick enough to lead to any enhanced energy transfer at the interface. We make this statement on the basis of the data presented in Figure 7, which demonstrate that the proton yield is largely dominated by the relative coverage and probability of depositing energy into the water clusters or aggregates vs the underlying substrate. Holes produced in or transferred to the water can migrate over distances which we estimate to be 1.0−1.2 nm. There does not appear to be efficient hole transfer from the substrate; however, efficient neutralization of holes on the chemisorbed water seems to occur. This can be seen by comparing Figure 6A and 6B. The water TPD in Figure 6B shows a strong feature between 200 and 275 K. However, the proton yield associated with this feature (Figure 6A) is rather small indicating that neutralization may be very efficient for this particular adsorbed state of water. This could result in a relatively high neutral atomic or molecular hydrogen yield. Thus, we are currently examining this possibility using resonance-enhanced multiphoton-ionization detection of the neutral atomic and molecular hydrogen products.

4. Conclusions

Electron-induced production and desorption of H^+, H_2^+, OH^+, and $H^+(H_2O)_n$ has been studied from water-covered zirconia surfaces. The proton yield is strongly dependent upon the type of water present with large yields mainly from ice aggregates or clusters. Proton formation and desorption occurs via 2-hole and 2-hole, 1-electron final states that are produced either directly or via Auger decay pathways. The increased yield with temperature is associated with structural and physical changes in the adsorbed water that includes disordering and increased excited-state lifetimes. The decreased yield is correlated with water desorption. Above 180 K, protons are produced by electron-stimulated dissociation of terminal hydroxyl groups present on the zirconia surface. At temperatures above 225 K, this yield drops and gives rise to electron-stimulated desorption of OH^+ ions. H_2^+ is also formed from adsorbed water and involves direct dissociative ionization. Some reactive scattering of energetic protons and 2-hole Coulomb interactions produce H_3O^+ and other higher mass clusters such as $H^+(H_2O)_n$, where $n = 2-8$. These clusters are minor products with low yields but are indicative of hole delocalization or screening distances.

The H^+ and H_2^+ yields dependence upon water coverage can be approximated using a model that accounts for the electron energy deposition probabilities within the overlayer vs the substrate. The present results on cation ESD from water-covered zirconia (~30 Å) thin films indicate efficient hole hopping within multilayers and ice clusters but not efficient interfacial energy exchange.

Acknowledgment. This work was carried out at Georgia Institute of Technology with equipment supplied by the United States Department of Energy (USDoE), Office of Science. The work was supported by the USDoE Nuclear Energy Research Initiative (NERI) under Grant No. DE-FG03-00SF22207. The authors also thank Mr. Matthew Gilliland for assistance during the initial stages of these experiments.

References and Notes

(1) Buchanan, R. C.; Pope, S. *J. Electrochem. Soc.* **1983**, *130*, 962.
(2) Loebs, V. A.; Haas, T. W.; Solomon, J. S. *J. Vac. Sci. Technol.* **1983**, *A1*, 596.
(3) Mansour, N.; Mansour, K.; Van Stryland, E. W.; Soileau, M. J. *J. Appl. Phys.* **1990**, *67*, 1475.
(4) Stichert, W.; Schuth, F. *J. Catal.* **1998**, *174*, 242.
(5) Tonkyn, R. G.; Barlow, S. E.; Orlando, T. M. *J. Appl. Phys.* **1996**, *80*, 4877.
(6) Sagert, N. H.; Robinson, R. W. *Can. J. Chem.* **1968**, *46*, 2075.
(7) Shishkina, E. A.; Kolomnikov, I. S.; Lysyak, T. V.; Rudnev, A. V. *Russian J. Inorg. Chem.* **1984**, *29*, 1223.
(8) Petrik, N. G.; Alexandrov, A. B.; Vall, A. I. *J. Phys. Chem. B* **2001**, *105*, 5935.
(9) LaVerne, J. A.; Tandon, L. *J. Phys. Chem. B* **2002**, *106*, 380.
(10) Petrik, N. G.; Alexandrov, A. B.; Orlando, T. M. *Trans. ANS* **1999**, *81*, 101.
(11) Orlando, T. M.; Meisel, D. *Nuclear Site Remediation*; ACS Symposium Series 778; American Chemical Society: Washington, DC, 2001; Chapter 17, p 284.
(12) Shuttanadan, V.; Thevuthasan, S.; Young, J. S.; Orlando, T. M.; Weber, W. J. *J. Nucl. Mater.* **2001**, *289*, 128. Maurice, V.; Salmeron, M.; Somorjai, G. A. *Surf. Sci.* **1990**, *237*, 116.

(13) French, R. H.; Glass, S. J.; Ohuchi, F. S.; Xu, Y.-N.; Ching, W. Y. *Phys. Rev. B* **1994**, *49*, 5133.
(14) Simpson, W. C.; Wang, W. K.; Yarmoff, J. A.; Orlando, T. M. *Surf. Sci*. **1999**, *423*, 225.
(15) Taylor, D. P.; Simpson, W. C.; Knutsen, K.; Henderson, M. A.; Orlando, T. M. *Appl. Surf. Sci.* **1998**, *127*−*129*, 101.
(16) Henderson, M. A. *Surf. Sci. Rep.* **2002**, *46*, 1.
(17) Takeuchi, K.; Perry, S. S.; Salmeron, M.; Somorjai, G. A. *Surf. Sci.* **1995**, *323*, 30.
(18) Maurice, V.; Takeuchi, K.; Salmeron, M.; Somorjai, G. A. *Surf. Sci.* **1991**, *250*, 99.
(19) Cerrato, G.; Bordiga, S.; Barbera, S.; Morterra, C. *Appl. Surf. Sci*. **1997**, *115*, 53.
(20) Nishino, Y.; Krauss, A. R.; Lin, Y.; Gruen, D. M. *J. Nucl. Mater*. **1996**, *228*, 346.
(21) Wang, Y. M.; Li, Y. S.; Mitchell, K. A. R. *Surf. Sci.* **1997**, *380*, 540.
(22) Maurice, V.; Salmeron, M.; Somorjai, G. A. *Surf. Sci.* **1990**, *237*, 116.
(23) Orlando, R.; Pisani, C.; Ruiz, E.; Sautet, P. *Surf. Sci*. **1992**, *275*, 482.
(24) Stirniman, M. J.; Huang, C.; Smith, R. S.; Joyce, S. A.; Kay, B. D. *J. Chem. Phys.* **1996**, *105*, 1295.
(25) Henderson, M. A. *Surf. Sci.* **1996**, *355*, 151.
(26) Souda, R. *Surf. Sci*. **2002**, *511*, 147.
(27) Noell, J. O.; Melius, C. F.; Stulen, R. H. *Surf. Sci.* **1985**, *157*, 119.
(28) Sieger, M. T.; Simpson, W. C.; Orlando, T. M. *Phys. Rev. B* **1997**, *56*, 4925.
(29) Sieger, M. T.; Orlando, T. M. *Surf. Sci.* **1997**, *390*, 92.
(30) Knotek, M. L.; Feibelman, P. J. *Phys. Rev. Lett.* **1978**, *40*, 964.
(31) Haglund, R. F.; Itoh, N. *Springer Ser. Mater. Sci.* **1994**, *28*, 11.
(32) Sieger, M. T.; Orlando, T. M. *Surf. Sci.* **2000**, *451*, 97.
(33) Penn, D. R. *Phys. Rev. B* **1976**, *13*, 5248.
(34) Ramaker, D. E. *Chem. Phys*. **1983**, *80*, 183.
(35) Tan, K. H.; Brion, C. E.; Van Der Leeuw, Ph. E.; Van Der Wiel, M. J. *Chem. Phys.* **1978**, *29*, 299.
(36) Richardson, P. J.; Eland, J. H. D.; Fournier, P. G.; Cooper, D. L. *J. Chem. Phys*. **1986**, *84*, 3189.
(37) Rottke, H.; Trump, C.; Sandner, W. *J. Phys. B: At. Mol. Opt. Phys*. **1998**, *31*, 1083.
(38) Rosenberg, R. A.; LaRoe, P. R.; Rehn, V.; Stohr, J.; Jaeger, R.; Parks, C. C. *Phys. Rev. B* **1983**, *28*, 3026.
(39) Souda, R. *J. Phys. Chem. B* **2001**, *105*, 5.
(40) Mitsui, T.; Rose, M. K.; Fomin, E.; Ogletree, D. F.; Salmeron, M. *Science* **2002**, *297*, 1850.
(41) Christensen, A.; Carter, E. A. *Phys. Rev. B* **1998**, *58*, 8050.